

CHARACTERIZING THE MORPHOLOGIES OF ENDOPLASMIC RETICULUM (ER) FROM STED IMAGES

Cameron Way (301370655), Dollina Dodani (301305914), Danilo Lekovic (301388110) and Saniya Ghorpade (301336699)

Department of Computing Science
Simon Fraser University, Burnaby BC, Canada
CMPT 340: Biomedical Computing
Dr. Ghassan Hamarneh
{cway, ddodani, dla188, sghorpad}@sfu.ca

Abstract. The Endoplasmic reticulum (ER) can adopt several morphologies depending on the cell type and functionality. Due to the components of the ER being highly dynamic, it has become increasingly essential to classify the two morphologies. Here, we present a comparative analysis of different methods based on using the multiscale second-order local structure of an image (Hessian) to characterize tubules from plate-like and blob-like morphologies. We performed an analysis based on distributions on the largest eigenvalues to select optimal thresholds for well-established vessel detection methods proposed previously. We tested and validated the selected optimum on a dataset of five stimulated emission depletion (STED) microscopy 2D and 3D images.

Keywords: Endoplasmic reticulum, morphology, vessel detection, Frangi filter.

1 Introduction

The endoplasmic reticulum (ER) is a membrane-bound organelle that spans throughout the cytoplasm. The ER can undertake different morphologies depending on the type of the cell and functions involved in protein and lipid synthesis. A network of interconnected tubules (tubes) and plate-like structures (sheets) stacked on top of each other are two well-characterized morphologies of the ER. While the structural theory of how the ER adopts different morphologies has not been established yet, it has become clinically essential to classify the two morphologies to detect the proteins produced in the cell. Several studies [8, 9] have attempted to characterize such structures; none have been able to validate and establish their proposed methods as a ground truth based on the biological interpretation of this problem.

In this report, we perform an analysis to select optimal thresholds for a method that relies on the second-order local structure (Hessian) of the provided sample stored as a TIF file. We leverage the k-largest eigenvectors (where k is the dimension of the image) derived from the Hessian matrix to classify the presence of each pixel in a tubular structure. This classification, based on suggested values for the two ratios (Ra and Rb) proposed by Frangi et al. and Descoteaux et al. We further use the distribution of the eigenvectors to select optimal thresholds for our classification models.

The rest of the report divides as follows: In section 2, the report covers the materials and samples along with the curation process used in this study; Sections 3 and 4 present the different methods (Frangi Filtering, KNN classifier, Closeness to Zero and Ra/Rb ratios), their appropriate thresholds, and their respective outcomes that identify the tubular structures; Section 5 states our accomplishments and obstacles we faced through the course of this project; Section 6 lists supervision received and contributions from each author; Section 7 concludes our study with suggested future work that could enhance the detection of different morphologies of the ER.

2 Materials

Our 2D and 3D analysis uses stimulated emission depletion (STED) microscopy images stored as TIF files. Each sample represented a cell under one of the two different protein expressions (G241 or HT1080) and their respective controls. We hypothesize that the morphology adopted is dependent on the protein expressed in the cell. The samples labelled as "control" would represent the morphology adopted by the ER in the absence of the interested protein. Our study received a total of 120 STED TIF files, randomly split into one of the four groups: G241 control, G241, HT1080 control, and HT1080.

2.1 Samples and Storage

There was a significant problem regarding the size of the data set. Images were hundreds of megabytes in size and, inherently loading said images was a slow process. Initially, we decided to run a compression algorithm, which decreased the image quality by 4x and utilized the Lempel-Ziv-Welch compression algorithm [3]. The Lempel-Ziv-Welch algorithm is a lossless data compression algorithm that is used in Unix-based systems to compress files [3]. As an example of the results, a 978.5 MB TIF file was compressed to 12.6 MB. Unfortunately, this created blurred and low-quality images shown in Figure 1. The results from merely cropping the images from the inside out removed the unnecessary space in the background and only sacrificed a little more storage space. In Figure 1, the same 978.5 MB image was cropped and compressed only using the L-Z-Q lossless algorithm, which resulted in a 34.8 MB image file. Unfortunately, this still reduced the quality of the image, so the processing steps of compression and cropping were eliminated.

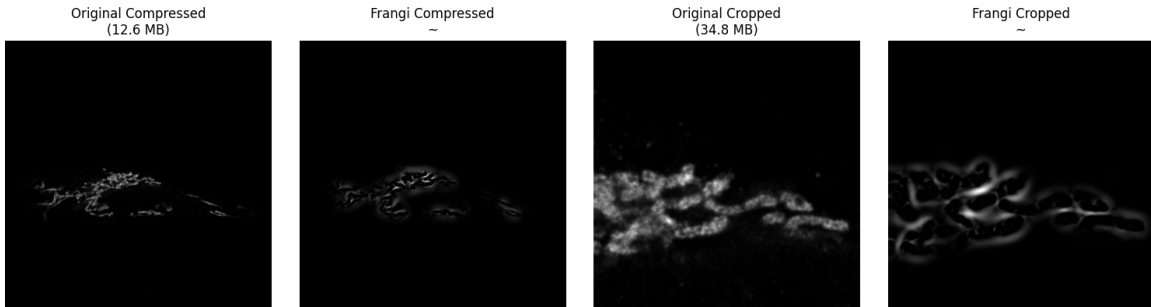


Figure 1. Compressed and cropped images.

2.2 Sample Curation

Due to low resolution and inciting background noise that generated erroneous characterization of structures, we eliminated 115 samples through manual curation. We visually examined each STED image to identify well-defined tubular and plate-like structures. While 20 samples passed initial quality checks, we settled on five due to limited computational resources available. These five samples are summarized in Table 1 and are available to download¹.

Table 1: Summary of the curated dataset

Sample ID	Cellular Environment	Number of frames
Decon_Series005_decon_z00_ch02	HT1080 Control	71
Decon_Series008_decon_z00_ch02	HT1080 Control	48
Decon_Series009_decon_z00_ch02	HT1080 Control	48
Decon_Series009_decon_z00_ch02	HT1080	63
Decon_Series010_decon_z00_ch02	HT1080	47

3 Methods

For classifying the morphologies of ER, it is common practice to apply a hessian filter over the image. The hessian matrix is composed of second-order partial derivatives of pixel values. The eigenvalues of the hessian matrix are a measure of concavity. There are k eigenvectors k dimensional (two for 2D and three 3D) hessian matrices. Once the concavity in each dimension is known, it is possible to determine the vessels and sheets of the region. In this report, the eigenvectors of the hessian matrix are represented by λ , and $|\lambda_1| < |\lambda_2| < |\lambda_3|$. Table 2 summarizes the conditions proposed by Frangi [1] to distinguish between tubes, sheets, noise and blobs. To algorithmically implement such thresholds, It became essential to have static thresholds to define high and low values. We deployed several methods in an attempt to generate these thresholds. These methods have been described in the following sections.

¹ <https://vault.sfu.ca/index.php/s/GbPAXWICEI4gCwX>

Table 2. Proposed structure descriptors for 3D eigenvalues assuming $|\lambda_1| < |\lambda_2| < |\lambda_3|$ (H = high, L = low)

λ_1	λ_2	λ_3	Structure
L	L	L	Noise
L	L	H	Sheet
L	H	H	Tube
H	H	H	Blob

3.1 Initial method

The initially proposed method to characterize the morphologies of the endoplasmic reticulum entailed the application of the vessel-enhancing Frangi filter and the analysis of Hessian matrix eigenvalues to determine characteristics at pixels. The Frangi filter and Hessian matrix were run on 2D image slices using the *sci-kit-learn* library. Eigenvalues were then obtained from the hessian matrix, analyzed, and classified based on the information shown in Table 2. Static thresholds for low and high were set to 10^{-12} and 10^{-7} , respectively. The pixels were marked as green representing tube-like regions and red representing sheet-like regions. This approach was overly sensitive, as shown in Figure 2.

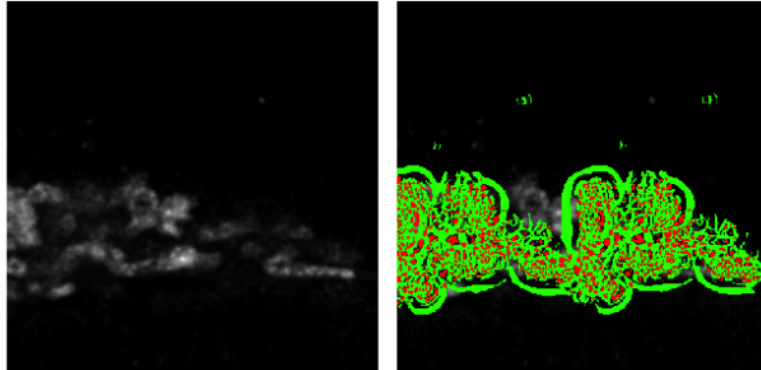


Figure 2. *Left:* unprocessed image with Frangi filter. *Right:* incorrectly highlighted regions.

3.2 Frangi/KNN

Given the sensitive nature of the initial method, we decided to combine it with K-Nearest Neighbors, an unsupervised learning algorithm. The KNN algorithm was extended and adapted from an open source project². This method uses a safe threshold that was selected by visual inspection of the eigenvalue distributions. This threshold is utilized by the initial method (as described in section 3.1), to classify the presence of each pixel in a tubular structure. This threshold forces Frangi to under-detect tubules and sheet structures and hence maintains a balance between sensitivity and specificity. This labelled image is then passed to the KNN implementation that considers 40 nearest pixels ($K=40$) to classify the pixel being analyzed.

3.3 Relative closeness to zero

After generating results from our 2D methods, we decided to implement a 3D method as we would be able to utilize information from three directions rather than trying to leverage only two eigenvectors. This led us to our initial 3D method, the relative closeness to zero method.

The relative closeness to zero method was intended to find the sheet regions by comparing λ_1 and λ_2 against λ_3 , the largest eigenvalue. Like the 2D methods, we used the Matlab code provided by D. Kroon [6], to calculate the Hessian matrix and eigenvalues in three dimensions. As described in Table 2, a sheet region can theoretically be found when λ_1 and λ_2 are low,

² <https://github.com/AbhinavUtkarsh/Image-Segmentation.git>

while λ_3 is high. The problem is that the terms ‘low’ and ‘high’ are relative, and therefore a threshold must be determined. For our algorithm, we used a threshold percentage of λ_3 to determine if λ_1 and λ_2 are close enough to zero (low). For instance if

$$|\lambda| < |0.4\lambda_3| \quad (1)$$

for both λ_1 and λ_2 , they would be considered ‘low’ and the region would be considered part of a sheet.

3.4 Ra/Rb Ratios

Frangi defines two ratios in his paper [2]. One being Rb, which measures how blob-like the structure is, and the other Ra is used to distinguish between sheet and tube structures. They are defined as:

$$Rb = \frac{|\lambda_1|}{\sqrt{\lambda_2 \lambda_3}} \quad Ra = \frac{|\lambda_2|}{|\lambda_3|} \quad (2)$$

These ratios in combination with the matrix norm make up the vesselness measure. We attempted to compute the vesselness measure in 3D, however, it did not produce any meaningful result using our data set. We then decided to decompose the vesselness function and use the Ra and Rb measures on their own. According to Frangi, tube like structures will have a Ra ratio equal to zero. However, in practice, the ratio will rarely be exactly equal to zero. For this reason, we must determine an acceptable interval for the threshold. We again started by determining thresholds manually through trial and error. Once we found a suitable threshold, we examined the histograms of Ra/Rb values throughout the image to try and spot a pattern.

4 Results

The following sections describe the results of a sample that best displays the characterization of tubules from sheets and blobs for the respective methods. These results can be extended to other samples in the curated dataset or any other TIF file of the STED microscopic modality.

4.1 Initial Method

The initial method produced our first acceptable results, however, this method was over-sensitive making it difficult to extrapolate to higher dimensions and other samples. The method required two thresholds that unless perfect, would over/under detect quite easily. The process of trying to find two good thresholds in this application is tedious to do manually, and difficult to do algorithmically. Figure 3 represents results generated from this method. The tubes were identified with a sensitivity of near 100%. However, a large portion of the sheet regions was incorrectly classified as tubes, thus reducing the specificity.

The original method was over-sensitive due to two reasons. First, the original images were relatively low-quality and did not clearly depict vessels nor sheets. This made it increasingly difficult to measure the accuracy of our results visually. Second, the output of the Frangi filter was passed to the hessian matrix function, causing it to over predict the tube regions. High-quality images were then selected for testing and produced the images seen in Figure 3. The resulting image (Figure 3: right) was still inaccurate and over detecting. After numerous threshold values were attempted, the resulting image remained highly sensitive and inaccurate.

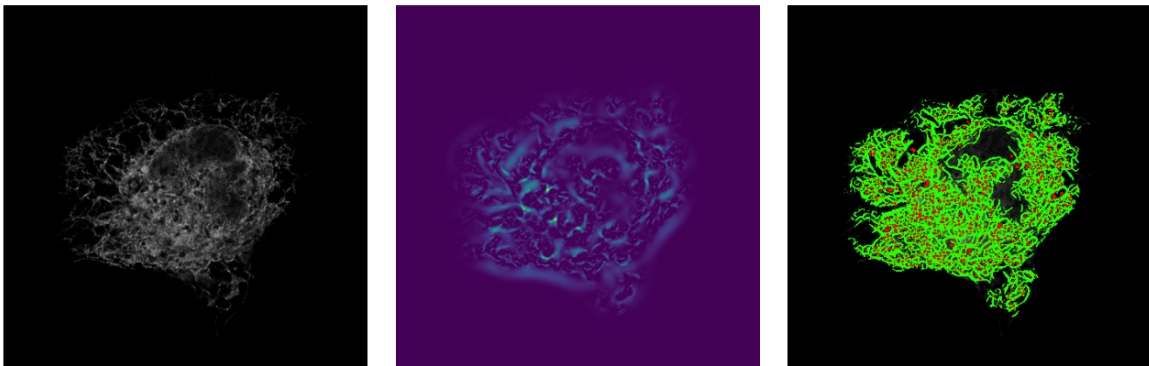


Figure 3. *Left:* original image. *Center:* image with Frangi filter applied. *Right:* image with more appropriate highlighting. This result is obtained from sample Decon_Series005_decon_z00_ch02 (HT1080 Control)

4.2 Frangi / KNN

Using the output of our original method as the input to KNN generated the results in Figure 4, where the tubular and sheet regions are indicated in grey and white, respectively. This method was a step in the right direction as it properly marked the tubular regions along the outer edge and suppressed background noise by only classifying pixels that belonged to ER. The area where the KNN method fell short is identifying the sheet regions accurately. These regions are often falsely predicted to be tubes when using this method just like our previous methods.

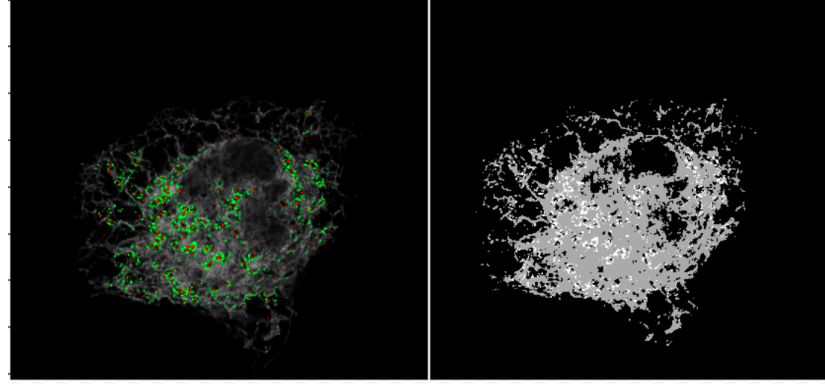


Figure 4. *Left:* image highlighted after ‘original method’ *Right:* image highlighted using ‘KNN’ after passed the image on left; This result is obtained from sample Decon_Series005_decon_z00_ch02 (HT1080 Control)

4.3 Relative closeness to zero

Relative closeness to zero was our first 3D method. With the extra dimension came more control over the conditions. We were now able to use information from all directions in order to classify the pixel. Because of the finer control over conditions, we were able to get results closer to what we were searching for. The tube regions are highlighted accurately, with a sensitivity near 100%, while ignoring much of the sheet regions, thus increasing specificity at the same time. This is a step above the KNN method which mispredicted much of the sheet regions. Unfortunately, the closeness to zero method was not effective for its designed purpose of detecting the sheet regions. We discuss the reason for this discrepancy in section 5.

4.4 Ra/Rb Ratios

The Ra/Rb ratios method was the closest to the vesselness filter that matched visual inspection, however we were unable to determine a method of programmatically determining the ideal threshold. Figure 5 shows one of our results that closely matched a classification done visually, and thus was relatively successful. For this image, we manually determined the threshold for which Ra and Rb were closest to the expected values. For instance, in Figure 5 we used thresholds $|Ra| < 0.4$ and $|Rb| > 0.4$ which provided the best results yet. This method proved to highlight the tubular regions while minimizing the number of sheets being misclassified as tubes and thus, was nominated as the method with the best results. We further tried to improve the results further by incorporating the R_{blob} ratio defined by Descoteaux [1] as

$$R_{blob} = \frac{|2\lambda_3 + \lambda_2 + \lambda_1|}{|\lambda_3|} \quad (3)$$

where if R_{blob} is equal to two, the pixel is classified as a sheet region. After much experimentation, we were unable to yield acceptable error tolerances to effectively integrate value from R_{blob} .

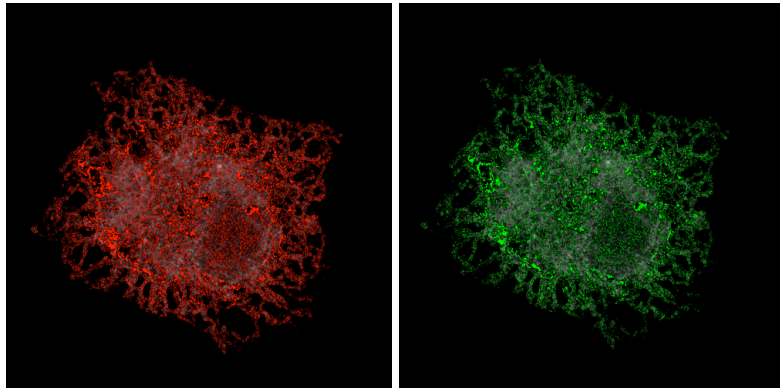


Figure 5. *Left:* Resulting slice from 3D ‘Closeness to zero’ method *Right:* Slice from 3D ‘Ra/Rb Ratios’ method
This result is obtained using sample Decon_Series008_decon_z00_ch02 (HT1080 Control)

5 Accomplishments

This project is an attempt to solve an intricate biological problem using sophisticated mathematical concepts. We aimed to identify relevant morphologies of the ER by using linear algebraic concepts of geometric shapes. This involved using the eigenvectors evaluated from the second-order local structure of the image (Hessian matrix). We deconstructed and extended prevalent vesselness filters such as the Frangi filter to set static thresholds for our purposes. We were able to use well-known ratios such as Ra and Rb to distinguish tubular structures from sheets and blobs in STED microscopic images stored as TIF files. A challenge that we encountered was to identify optimal thresholds for these ratios to generate accurate results.

While Frangi et al.’s study provided expected values for each ER morphology, we found that those values were not generalizable and did not fit our dataset. After some testing, we realised our eigenvalues did not have the consistent pattern like the ones proposed by Frangi et al. in Table 2. This significantly hindered our progress as we could not follow the ratios, formulas and conventions developed by Frangi [2] and Descanteaux [1]. We tried to circumvent this issue by introducing error tolerances, analyzing the distribution of eigenvectors, and rigorous experimentation of different thresholds. The inconsistent pattern of eigenvalues ultimately made it difficult to get consistent results.

Another major obstacle that we faced while working on our project was deploying a deep-learning framework for ER classification. After initial quality checks, the curated dataset contained 5 samples which were restrictive for implementation of the U-NET framework. In addition to a small sample size and challenges associated with manually annotating regions of interest, we were unable to apprehend the parameters that needed to be fine-tuned for our dataset due to our limited expertise in deep learning.

Lastly, we had an issue with the size of our dataset. The original dataset was over 50GB, meaning most of our group was unable to download and view all of the samples. To remedy this issue, one member picked a few of the clearest samples to share with the rest of the group. The other issue with such large images is that they take a long time to process. We ran into a number of issues with algorithm efficiency. For this reason, when processing the 3D images using our filters, we could only process around ten slices at a time.

Through this project, we have been able to bridge the gap between biological and quantitative sciences that could be leveraged to advance health care and improve patient treatment. We have come to understand the significance of being able to find resources, deconstruct complicated mathematical notation from published scientific papers, and adapt them for our research. We have also learned to be critical of our results and measure them by using concepts of sensitivity and specificity.

6 Contributions

Dr. Hamarneh was instrumental in providing the project idea and data. He also provided resources to published algorithms that have been extended and adapted in the following ways by the authors:

Cameron’s Contributions: Cameron tested the Matlab Frangi Filter code and attempted to extend it to our purposes. After the Matlab code proved to be too slow for reasonable use, he extended Danilo’s python ‘highlight’ function to highlight the images in 3D, using the D. Kroon’s [6] Matlab code. Cameron, along with Dollina tried to implement several different tubule and sheet region conditions including using Frangi’s vesselness measure. When that did not produce proper results, they

deconstructed the vesselness function and manipulated the Ra and Rb ratios on their own to produce better results, as well as implemented the relative closeness to zero method in python. Cameron also manually curated the dataset to identify high-resolution images.

Dollina's Contributions: Dollina started this project testing the U-net functionality with Saniya. When the U-net portion of our project was ultimately eliminated, due to computational requirements, Dollina helped create histograms of the eigenvalues to try and shed some light on our threshold issue. She and Cameron implemented the relative closeness to zero and Ra/Rb methods. Dollina further adapted the implementation of KNN to study the combined effect of the Frangi filter along with an unsupervised algorithm.

Danilo's Contributions: Danilo had a large part in getting the initial algorithm containing the highlight function set up. He wrote the code for our initial method using the Frangi filter and the eigenvalues of the hessian matrix. He also set up the graphical interface for the program. Danilo tried several different thresholding methods. Danilo also contributed to the initial curation of the dataset and helped compress images for effective distribution of data to the group.

Saniya's Contributions: Saniya also worked on the U-net part of this project during the first part of this project. Once this part was abandoned, she helped with trying to determine the proper thresholding method for our algorithms.

7 Conclusion & Discussions

This project involved the application of the Frangi filter to establish the classification of ER morphologies based on the overexpression of certain proteins. Several different approaches were tested to generate thresholds to distinguish between tubes from sheets and blobs. The initial analysis observed the application of Frangi filter on 2D image slices along with the Hessian matrix for eigenvalue computation. This method being overly sensitive, resulted in erroneous highlighting of the ER regions. Partially accurate classification of tubes and sheets was achieved through experiments on threshold values. The second method entailed the application of the KNN classifier on the labelled image generated from the initial method. The KNN algorithm classified each pixel based on its proximity to k-neighboring pixels but lead to overfitting results for the tubular region. In computing the relative closeness to zero method, λ_1 and λ_2 are compared to λ_3 . A threshold obtained through trial and error is used to distinguish between 'low' and 'high' eigenvalues. The closeness to zero method was initially designed to detect sheets but was ineffectual. The last method uses Ra/Rb ratios to give a measure for the vesselness of the image. Each of the methods is utilized for a different goal of classification and while some give accurate results, the others are difficult to accomplish further.

Since our study relies heavily on the Ra and Rb ratios suggested by Frangi et al, our analysis inherits limitations of their methods. One such limitation is the rise of artifacts in transition steps of the Frangi filter [2] which leads to a reduction of the measured signal in the fourier domain. This is also observed in Figure 3 centre, which shows reduced signal after the application of the filter. While Frangi et al.'s method utilizes information from all axes by operating on the k eigenvectors for each pixel (where k is the dimension of the image - two for 2D and three for 3D), other studies [7] perform vessel segmentation with a few selected eigenvectors from k vectors. This method of selecting a subset of eigenvectors has not been tested and validated in this work and thus warrants further investigation.

7.1 Future Work

In this report, we have focused on the characterization of tube-like structures from sheets and blobs. We have leveraged the proposed algorithms by Frangi et al. and Descoteaux et al., and manually found optimal thresholds to perform characterization of such line structures. The proposed method relies on the distribution of two or three largest eigenvalues that have been generated using the second-order local structure of the image to select an optimal static threshold. While the results discussed above can detect tubular structures, it has an immensely high sensitivity, thus warranting further study. In the future, we aim to automate the process of selecting an appropriate threshold given a sample, generalize the process to all the frames for a provided 3D image, and leverage vesselness measure[2] to increase the specificity of our model. In the light of recent advances and progress made in machine learning for image classification, we aspire to deploy and extend a deep learning framework that would be trained on manual annotations of tubular and plate-like structures. Such a model would depend on a large cleaned dataset of single modularity, hence making it difficult to implement. Given more time, we would focus more time on increasing the efficiency of our program by using element-wise operations over loops.

Acknowledgements

We would like to thank Dr. Ghassan Hamarneh for his support in helping us understand the significance of this problem, for providing us with the STED images, and for pointing us to published algorithms that have been leveraged in this report. We would also like to extend our gratitude to Kathleen Moriarty for her guidance which helped us solidify the objective of our project.

References

1. Descoteaux, Maxime, et al. "Bone enhancement filtering: application to sinus bone segmentation and simulation of pituitary surgery." *Computer aided surgery* 11.5 (2006): 247-255.
2. Frangi, Alejandro F., et al. "Multiscale vessel enhancement filtering." *International conference on medical image computing and computer-assisted intervention*. Springer, Berlin, Heidelberg, 1998.
3. Indiana University. "What is LZW and what are the issues surrounding it?" *Knowledge Base* (2018).
4. Jin, Jiaoying, et al. "Vascular tree segmentation in medical images using Hessian-based multiscale filtering and level set method." *Computational and mathematical methods in medicine* (2013).
5. Longo, Antonia, et al. "Assessment of hessian-based Frangi vesselness filter in optoacoustic imaging." *Photoacoustics* 20 (2020): 100200.
6. Dirk-Jan Kroon (2021). Hessian based Frangi Vesselness filter (<https://www.mathworks.com/matlabcentral/fileexchange/24409-hessian-based-frangi-vesselness-filter>), MATLAB Central File Exchange. Retrieved April 25, 2021.
7. Sato, Yoshinobu, et al. "Three-dimensional multi-scale line filter for segmentation and visualization of curvilinear structures in medical images." *Medical image analysis* 2.2 (1998): 143-168.
8. Papagiannidis, Dimitrios, et al. "Ice2 promotes ER membrane biogenesis in yeast by inhibiting the conserved lipin phosphatase complex." *BioRxiv* (2021): 2020-02.
9. Shemesh, Tom, et al. "A model for the generation and interconversion of ER morphologies." *Proceedings of the National Academy of Sciences* 111.49 (2014): E5243-E5251.